Chemical Engineering Journal (2015). 264, 497-505.
DOI: http://dx.doi.org/10.1016/j.cej.2014.11.107

Energy storage with PCM in fluidized beds: modeling and experiments

M.A. Izquierdo-Barrientos[a,*], C. Sobrino[a], J.A. Almendros-Ibáñez[b,c]

[a] *Universidad Carlos III de Madrid, ISE Research Group, Thermal and Fluid Engineering Department, Avda. de la Universidad 30, 28911 Leganés, Madrid, Spain*
[b] *Escuela de Ingenieros Industriales, Dpto. de Mecánica Aplicada e Ingeniería de Proyectos, Castilla-La Mancha University, Campus universitario s/n, 02071, Albacete, Spain*
[c] *Renewable Energy Research Institute, Section of Solar and Energy Efficiency, C/ de la Investigación s/n, 02071, Albacete, Spain*

Abstract

In recent years, the development of phase change materials (PCMs) has introduced new ways to increase the energy storage capacity of a system due to the high latent heat and high storage density of these materials. The aim of this work is to model the charging process of a fluidized bed with PCMs operating as an energy storage device. The temperature in the bed during the charging process of the fluidized bed has been modeled using the two phase theory of fluidization. The dense phase is taken to be perfectly mixed, and the bubble phase is taken to be in plug flow. The numerical model presented takes into account the fact that the phase change process of the bed material occurs over a temperature range and also estimates the energy stored in the wall of the bed and in the distributor plate. The energy equation of the dense phase is numerically solved in enthalpy form, considering the depen-

*Corresponding author. Tel.:+34 91 624 83 71
Email address: maizquie@ing.uc3m.es (M.A. Izquierdo-Barrientos)

dence of enthalpy on temperature for phase changes occurring over a range of temperatures. The model's validity is verified against experimental data for two granular materials: sand, a typical material used in fluidized beds, and a granular PCM with a mean particle diameter of 0.54 mm and a phase change temperature of approximately 50°C. For the sand, the temperature profiles obtained numerically perfectly agree with the values measured experimentally. In the case of the granular PCM, the fitting of the curves is improved when slow and similar heating rates are selected for the experiments and for the DSC measurements used to determine the PCM enthalpy-temperature curve.

Keywords: Fluidized bed, Phase change material, Energy storage, Heat transfer

1. Introduction

Time-dependent energy resources require effective storage methods to reduce the mismatch between supply and demand. Sensible heat storage is the most common method of thermal storage, although the latent heat method provides a much higher energy storage density with small temperature swings. Due to these advantages, much research has been focused on studying, theoretically and experimentally, the performance of energy storage methods employing phase change materials (PCMs), especially regarding their application in packed beds [1, 2, 3]. Compared with packed beds, fluidized beds have the advantage of a higher rate of heat transfer between the carrying fluid and the storage medium, as well as presenting a uniform temperature along the bed.

In spite of the advantages of fluidized beds over fixed beds, only a few studies have examined fluidized beds as heat storage devices. Elsayed et al. [4] tested an air-sand fluidized bed for thermal storage, in which the bed was heated or cooled by a flow of air. They observed that the bed always behaves as a well mixed tank. Sozen et al. [5] presented an experimental investigation using 25-mm-diameter PCM spheres in a water fluidized bed, showing that with cycling, fluidization yielded less of a loss in heat storage efficiency than was observed under fixed bed conditions. Izquierdo-Barrientos et al. [6] presented heating experiments using a granular PCM of 0.54 mm mean diameter in an air fluidized bed, obtaining higher charging efficiencies than in sand beds and stable behavior after 75 hours of continuous operation.

The unsteady state behavior of fluidized bed thermal storage systems has been modeled in a limited number of studies in the literature, and only for sensible heat. Wagialla et al. [7] used the two phase theory of fluidization to simulate the transient response of a bed of alumina particles fluidized by a hot air stream and verified the results with experimental data. They neglected the energy stored in the bubble phase, which made it possible to obtain an analytical expression for the bubble phase temperature. A similar model developed by El-Halwagi et al. [8] was used to study the influence of different parameters (gas flow rate, mass of solids and bed aspect ratio) on the performance of the system as a heat regenerator.

In this paper, a model for the transient response of a fluidized bed containing PCM is presented and verified by experimental measurements. The fluidized bed is modeled using the two phase theory of fluidization, assuming that the emulsion phase is perfectly mixed and assuming plug flow in the

bubble phase. It is assumed that all gas in excess of what is required for minimum fluidization passes through the bed as bubbles, which exchange heat with the dense phase as they rise. The energy equation for the emulsion phase is calculated employing the enthalpy method, given that the phase transition occurs over a temperature range [9]. The heat accumulated in the stainless steel vessel and in the plate distributor is included in the simulations.

Previous results from the work of Kunii and Levenspiel [10], who proposed a correlation for the heat transfer coefficient from the bubble phase to the emulsion phase are used in this work. The modelization of the heat transfer coefficient between a fluidized bed and an external wall has been subject of many studies. However, this coefficient depends on local hydrodynamic information, which makes difficult its use for different particles and flow conditions [11]. In this paper, the work of Izquierdo-Barrientos et al. [12], who measured and modeled the heat transfer coefficient to an immersed surface in bubbling fluidized beds of sand and granular PCM, is used.

2. Materials and experimental apparatus

Heating experiments for sand and a PCM in a fluidized bed have been carried out to validate the model proposed in this study. Figure 1 shows a schematic of the set up. It consists of a cylindrical stainless steel bed with a 2 mm wall thickness filled with particles. The air enters the plenum of the column and then flows into the bed through a 1.5-mm-thick distribution plate with 300 orifices with a 2 mm diameter, resulting in an open area of 3%. The distributor has been designed to have a pressure drop equal to 30% of the bed pressure drop [15]. In this way, the air is uniformly distributed in the

bed. A fine-mesh screen is mounted at the bottom of the distributor plate to prevent solid particles from entering the plenum chamber. The instrumental test section is 500 mm in height, has an internal diameter of 200 mm and is insulated with glass wool with a thickness of 2 cm. The piping is insulated with a 1-cm-thick thermal insulator. The freeboard of the column is divided into two parts, one cylinder with an internal diameter of 200 mm and another with an internal diameter of 300 mm. The purpose of this division is to assure a homogeneous velocity distribution of air at the exit from the test section and to reduce the elutriation and entrainment of particles from the bed.

[Figure 1 about here.]

The air flow is produced by a blower with a variable mass flow rate and is heated by electrical heaters before flowing to the column. For the PCM experiments, the column is filled with 5 kg of PCM, whereas 7.25 kg is used for the experiments with sand. The fixed bed height is $H = 200$ mm for all the experiments. Type K thermocouples are used to measure the temperature at specific locations inside the test section. Air temperature is also measured at the inlet and outlet of the test section. These thermocouples are connected to a data acquisition system for continuous monitoring and recording of the data.

The materials used for the experiments are sand and a granular phase changing composite (Rubitherm®-GR50), with a phase change temperature T_{pc} interval of 45-51°C, according to the manufacturer. Both the sand and the GR50 material correspond to group B of Geldart's classification [16]. This means that they fluidize easily with vigorous bubbling action and that the bubbles grow large [15].

Table 1 gives several properties of the sand and PCM, such as density ρ, thermal conductivity k, mean particle diameter $\overline{d}_p$ and standard deviation σ_{dp}, and minimum fluidization velocity U_{mf}. Moreover, the variation of specific heat with the temperature obtained by differential scanning calorimetry (DSC) is plotted for each material in Figure 2(a). These data are obtained with a heating rate of 0.5°C/min [17]. For the PCM, the curve of the specific heat versus temperature shows a clear peak between 40 and 50°C, where the phase change process occurs. By contrast, the curve for the sand is approximately linear with an average value of $c_p = 0.7$ kJ/(kg·K) in the range of temperatures shown in Figure 2(a). In addition, the variation of enthalpy with temperature for the PCM is presented in Figure 2(b). Both materials have a similar mean particle size, although the density of the GR50 is approximately half that of the sand. Consequently, the minimum fluidization velocity of the GR50 is 0.13 m/s, much lower than that of the sand (0.27 m/s).

[Table 1 about here.]

[Figure 2 about here.]

3. Heat transfer model in a fluidized bed

In the following sections, the two phase fluidized model is described. First, the model is explained for a fluidized bed without a phase change in the granular material; then, the modifications needed in the emulsion phase to include the phase change are explained.

3.1. Fluidized bed model without phase change in the dense phase

The two phase model considers a fluidized bed as a bubble phase and a surrounding suspension phase consisting of solid particles and gas, known as the dense or emulsion phase. The energy conservation equations are based on a heat balance involving the dense phase (assuming a uniform temperature), a differential element in the bubble phase (assuming plug flow) and the container walls

The heat accumulated in the dense phase is equal to the net enthalpy flow of the fluidizing gas (which is assumed to leave the bed at the dense phase temperature), the heat transferred from the dense phase to the bubble phase and the heat transferred from the dense phase to the container walls [7]. Following this statement, the heat balance for the dense phase is expressed as

$$\begin{aligned}(\rho_a\,\varepsilon\,c_{p,a}+\rho_s\,(1-\varepsilon)\,c_{p,s})A_d\,H\,\frac{\partial T_d}{\partial t} &= G_d\,\rho_a\,c_{p,a}\;(T_{in}-T_d)+\\ +\int_0^H P_b\,h_b\,(T_b-T_d)\,dx &+ A_{wi}\,h_w(T_w-T_d),\end{aligned} \tag{1}$$

where T_d is the dense phase temperature, T_b is the bubble phase temperature, T_w is the container wall temperature, T_{in} is the gas temperature at the inlet of the bed, H is the bed height, ε is the voidage in the bed, A_d is the cross sectional area of the dense phase, A_{wi} is the internal surface area of the container wall, P_b is the perimeter of the cross sectional area of the bubbles and h_b is the convective heat transfer coefficient between the bubbles and the dense phase. The volumetric flow rate through the dense phase $G_d = A\,U_{mf}$ has been calculated by assuming that the dense phase remains at minimum

fluidization conditions while all gas in excess of U_{mf} passes through the bed as bubbles.

The convective heat transfer coefficient between the dense phase and the container wall, h_w, has been calculated using the model proposed by Izquierdo-Barrientos et al. [12, 13]. This model has been tested with the same materials (sand and granular PCM) and experimental conditions of this work and it is explained in deep in [13]. In addition, this model has been compared with different experimental results of other researchers under different fluidization conditions [14].

The heat transfer coefficient from the bubbles to the dense phase h_b has been calculated from the total heat interchange across the bubble cloud boundary per unit of bubble phase [15]:

$$H_{bc} = 4.5 \left(\frac{U_{mf}\, \rho_a\, c_{p,a}}{d_b} \right) + \frac{5.85 \left(k_a\, \rho_a\, c_{p,a} \right)^{1/2}\, g^{1/4}}{d_b^{5/4}}, \tag{2}$$

where g corresponds to gravity and d_b is the diameter of a sphere with the same volume as the spherical cup bubble calculated by finding the average value of the expression presented by Darton et al. [18] along the bed height. The first term of Equation (2) corresponds to transfer by bulk gas flow and the second to transfer by convection. Under the experimental conditions of this work, the latter term is almost one order of magnitude lower than the former.

Using correlation (2), the heat transfer coefficient from the bubble phase to the dense phase per unit length $P_b\, h_b$ that appears in the second term on

the right hand side of Equation (1) can be calculated as

$$P_b h_b = \frac{S_b}{H} \frac{H_{bc} V_b}{S_b}, \tag{3}$$

where S_b is the bubble surface and V_b corresponds to the bubble volume. Using the expression $\delta = V_b/V = A_b/A$, where V is the bed volume, Equation (3) can be rewritten as

$$P_b h_b = H_{bc}\, \delta\, A. \tag{4}$$

The parameter δ corresponds to the volume fraction of the bed in bubbles, which, according to the two phase model, can be calculated as

$$\delta = \frac{U - U_{mf}}{U_b}, \tag{5}$$

where U is the superficial gas velocity and U_b is the rising velocity of bubbles given by the expression [19]

$$U_b = U - U_{mf} + 0.711\, (g\, d_b)^{1/2}\,. \tag{6}$$

The heat balance for a differential element of the bubble phase yields the equation

$$A_b \rho_a\, c_{p,a} \frac{\partial T_b}{\partial t} = -G_b\, \rho_a\, c_{p,a} \frac{\partial T_b}{\partial x} + P_b\, h_b\, (T_d - T_b)\,, \tag{7}$$

where A is the cross sectional area of the bed, $A_b = A\delta$ is the cross sectional area of the bubble phase and $G_b = A\,(U - U_m f)$ is the volumetric flow rate through the bubble phase. In this way, the heat accumulated in a bubble phase element is equal to the net enthalpy flow of the fluidizing gas and the heat interchanged with the dense phase.

The heat accumulated in the wall of the bed is defined as the heat transferred by the dense phase and the heat lost to the ambient surroundings, leading to

$$\rho_w\, c_{p,w}\, A_w\, H_w \frac{\partial T_w}{\partial t} = A_{wi}\, h_w\, (T_d - T_w) + A_{wo}\, U_{wo}\, (T_0 - T_w)\,, \tag{8}$$

where T_0 is the ambient temperature, A_w is the cross sectional area of the container wall, H_w is the height of the wall and U_{wo} is the global heat transfer coefficient between the container wall and the ambient surroundings.

The boundary and initial conditions used to solve the differential equation system formed by Equations (1), (7) and (8) are summarized in Table 2.

[Table 2 about here.]

The proposed differential equation system can be transformed into a non-dimensional system by introducing the following non-dimensional variables:

$$\hat{T}_d = \frac{T_d - T_0}{T_{max} - T_0}, \quad \hat{T}_b = \frac{T_b - T_0}{T_{max} - T_0}, \quad \hat{T}_w = \frac{T_w - T_0}{T_{max} - T_0},$$
$$\hat{T}_{in} = \frac{T_{in} - T_0}{T_{max} - T_0}, \quad \hat{t} = t\,\frac{U}{\varepsilon\, H}, \quad \hat{x} = \frac{x}{H}.$$

With this change, the non-dimensional temperatures vary between 0, when the temperature is equal to the ambient temperature (minimum temperature) T_0, and 1, when the temperature is equal to T_{max}, which is the

maximum temperature of the introduced air. As a result, the original system takes the form

$$\frac{\partial \hat{T}_d}{\partial \hat{t}} = \hat{U}_d R_{a-s} \left(\hat{T}_{in} - \hat{T}_d\right) + \int_0^1 St_{b-s} \left(\hat{T}_b - \hat{T}_d\right) d\hat{x} + St_{wi-s} \left(\hat{T}_w - \hat{T}_d\right), \tag{9}$$

$$\frac{\partial \hat{T}_b}{\partial \hat{t}} = -\hat{U}_b \varepsilon \frac{\partial \hat{T}_b}{\partial \hat{x}} + St_{b-a} \left(\hat{T}_d - \hat{T}_b\right), \tag{10}$$

$$\frac{\partial \hat{T}_w}{\partial \hat{t}} = St_{wi-w} \left(\hat{T}_d - \hat{T}_w\right) + St_{wo-w} \left(\hat{T}_0 - \hat{T}_w\right), \tag{11}$$

where St represents different Stanton numbers, $\hat{U}_b$ is the dimensionless superficial velocity of the bubble, $\hat{U}_d$ is the dimensionless velocity of the dense phase and R_{a-s} is the ratio of the volumetric heat capacities of the air and the solids, defined as

$$St_{b-s} = \frac{P_b\, h_b\, H\, \varepsilon}{\rho_s\, (1-\varepsilon)\; c_{p,s}\, A_d\, U}, \quad St_{wi-s} = \frac{A_{wi}\, h_w\, \varepsilon}{A_d\, (1-\varepsilon)\; \rho_s\, c_{p,s}\, U},$$
$$St_{b-a} = \frac{P_b\, h_b\, H\, \varepsilon}{A_b\, \rho_a\, c_{p,a}\, U}, \quad St_{wi-w} = \frac{A_{wi}\, h_w\, H\, \varepsilon}{A_w\, \rho_w\, c_{p,w}\, U\, H_w},$$
$$St_{wo-w} = \frac{A_{wo}\, U_{wo}\, H\, \varepsilon}{A_w\, \rho_w\, c_{p,w}\, U\, H_w}, \quad \hat{U}_b = \frac{G_b}{A_b\, U},$$
$$R_{a-s} = \frac{\varepsilon\, \rho_a\, c_{p,a}}{(1-\varepsilon)\; \rho_s\, c_{p,s}}, \quad \hat{U}_d = \frac{G_d}{A_d\, U}.$$

The initial and boundary conditions in non-dimensional form are included in Table 3.

[Table 3 about here.]

3.2. Fluidized bed model with phase change in the dense phase

When the dense phase contains granular PCM whose phase change occurs over a temperature range, the phase change process can be introduced using an apparent specific heat, which is a function of temperature (Figure 2(a)) Thus, the energy equation of the dense phase for a conventional granular material (Equation (1)), neglecting the heat capacity of the gas in comparison with the heat capacity of the solid, is transformed into

$$\rho_s \left(1-\varepsilon\right) A_d L \frac{\partial i_d}{\partial t} = G_d \rho_a \, c_{p,a} \, \left(T_{in} - T_d\right) + \int_0^H P_b h_b \left(T_b - T_d\right) dx + A_{wi} \, h_{wi} \left(T_w - T_d\right), \tag{12}$$

where i_d represents the enthalpy of the solid.

Equation (12) can be non-dimensionalized by introducing the dimensionless variable enthalpy

$$\hat{i}_d = \frac{i_d - i_{d_0}}{\bar{c}_{p,s} \left(T_{max} - T_0\right)} = \int_0^{\hat{\theta}} \hat{c}_{p,s} \, d\hat{\theta}, \tag{13}$$

where

$$\bar{c}_{p,s} = \frac{1}{T_{max} - T_0} \int_{T_0}^{T_{max}} c_{p,s} \, d\theta \tag{14}$$

is the average apparent specific heat in the range of temperatures of the experiments and

$$\hat{c}_{p,s} = \frac{c_{p,s}}{\bar{c}_{p,s}} \tag{15}$$

is a non-dimensional specific heat defined as the ratio of the specific heat at a certain temperature and the average specific heat defined previously. Using the non-dimensional variables, Equation (12) is converted into the non-dimensional

$$\frac{\partial \hat{i}_d}{\partial \hat{t}} = \hat{U}_d \overline{R}_{a-s} \left(\hat{T}_{in} - \hat{T}_d \right) + \int_0^1 \overline{St}_{b-s} \left(\hat{T}_b - \hat{T}_d \right) d\hat{x} + \overline{St}_{wi-s} \left(\hat{T}_w - \hat{T}_d \right) \quad (16)$$

where $\hat{U}_d$, $\overline{R}_{a-s}$, $\overline{St}_{b-s}$ and $\overline{St}_{wi-s}$ are the dimensionless numbers defined before where $\hat{U}_d$, $\overline{R}_{a-s}$, $\overline{St}_{b-s}$ and $\overline{St}_{wi-s}$ are the previously defined dimensionless numbers, in which the constant specific heat of the sand $c_{p,s}$ is replaced by the average specific heat of the PCM, $\overline{c}_{p,s}$, defined in Equation (14).

The energy balance presented in Equation (9) has the same structure as Equation (16), but the latter is described as a function of enthalpy. Thus, for each time step, values for $\hat{i}_d$ are calculated, and then the temperature of the dense phase T_d is determined from the calculated enthalpy using the specific heat function obtained with the DSC (Figure 2(a)). Therefore, the numerical method used to solve the system of equations is the same, even though there is a phase change in the granular material.

3.3. Numerical solution for the heat transfer model

The system of differential equations formed by Equations (9), (10) and (11) for the conventional granular material, sand, or by Equations (10), (11) and (16) for the granular PCM can be numerically solved by an explicit finite difference technique. The results are obtained with a spatial step of $\Delta x = 1$ cm and a temporal step of $\Delta t = 0.2\Delta x \varepsilon / U$, which ensures the convergence of the numerical method. The temporal derivatives are approximated by the

fourth-order Runge-Kutta method, and the spatial derivatives are approximated using an up-wind scheme.

When the solid enthalpy is obtained from Equation (16), the solid temperature is obtained from Figure 2(b). The data represented in this Figure have been interpolated using cubic spline interpolation.

4. Results

Figure 3 illustrates the evolution of the experimental and numerical temperatures for the sand. The selected flow rate is $G_{1,sand}$= 1000 l/min, which corresponds to an excess air velocity over minimum fluidization conditions of approximately $U/U_{mf} = 2$. The ambient temperature is $T_0 = 18$°C. The temperature of the feed gas differs from that of the gas that leaves the distributor plate and enters the bed, and hence the influence of the distributor plate needs to be considered. This fact has been observed by other researchers [20, 21]. The influence of the distributor plate has been characterized experimentally in this work, and the temperature difference between the gas at the plenum chamber and at the bed inlet, after the distributor plate, has been measured in the empty vessel at different gas flow rates. This temperature difference has been subtracted from the temperature measured in the plenum chamber T_{plenum} to estimate the value of the inlet air temperature for the different cases studied, which corresponds to T_{in} in the graphs. The global heat transfer coefficient U_{wo} is 3 W/m^2·K. This parameter has been calculated as the value that satisfies the steady state temperature of the bed and is suitable for all the flow rates used. The heat transfer coefficient between the bed and the container wall for this case is $h_w = 894$ W/(m^2 K) and the heat inter-

change between the bubble and the dense phase $H_{bc} = 3.44 \times 10^4\,\mathrm{W/(m^3\,K)}$. The values of these coefficients are summarized in Table 4 for the two materials and for the different gas flow velocities used in this work. It has been confirmed that variations of 10% of these heat transfer coefficients do not affect the temperature profiles modeled.

[Table 4 about here.]

Because of the plug flow behavior of the bubble phase, its temperature evolution T_b is plotted at different heights: $x = 3$ cm, $x = 5$ cm and $x = 7$ cm. Above a bed height of 10 cm, there is nearly no difference between the bubble and dense phase temperatures. As expected, the system behaves as a well mixed tank, and the dense phase temperature T_d is uniform along the bed height. The experimental temperature of the dense phase T_{exp} is measured along the axis of the bed at three different heights. Because the values of T_{exp} at different heights are the same, only one of the temperature profiles is plotted in the subsequent figures.

From the results in Figure 3, it can be concluded that there is good agreement between the experimental and numerical data for the dense phase.

[Figure 3 about here.]

The same experiments have been performed at different flow rates, $G_{2,sand} =$ 700 l/min and $G_{3,sand} = 875$ l/min, which correspond to excess air velocities over a minimum fluidization of approximately $U_{2,sand} = 1.5\,U_{mf}$ and $U_{3,sand} = 1.75\,U_{mf}$. The results are plotted in Figure 4(a) and 4(b), showing analogous behavior to the case previously presented. The temperature of the

dense phase predicted by the model is adjusted properly to the experimental measurements. The temperature of the wall vessel follows the temperature of the dense phase with a small delay.

[Figure 4 about here.]

Figure 5 shows the numerical and experimental results obtained for the bed filled with granular PCM when the flow rate corresponds to $G_{1,PCM} =$ 500 l/min ($U_{1,PCM} = 2\,U_{mf}$). The coefficient U_{wo} varies between 0.77 and 6 W/m^2·K, depending on the air flow rate. The same uniform behavior is observed in the dense phase as is observed for sand, with a homogeneous temperature along the bed. Furthermore, the phase change process is clearly reflected in the change in slope of the curves near the phase change temperature interval of (40-50°C). In this case, there are discrepancies between the experimental and numerical data, especially during the phase change process. These discrepancies are attributed to the difference between the heating rate of the material during the experiment, which is approximately 1.5°C/min, and the rate used during the DSC measurements, 0.5°C/min, to obtain the enthalpy-temperature curve used in the model (Figure 2). Rady [17] found that high heating rates promote the development of thermal non-equilibrium effects inside the sample material and result in an increase in the temperature range for melting. It is also observed that the shape of the enthalpy variation curve with temperature depends on the heating rate, calling for functions derived for heating rates similar to those experienced in the actual application.

[Figure 5 about here.]

Two more experiments have been carried out for the flow rates $G_{2,PCM} = 375$ l/min and $G_{3,PCM} = 625$ l/min, which correspond to excess air velocities over minimum fluidization of approximately $U_{2,PCM} = 1.5\,U_{mf}$ and $U_{3,PCM} = 2.5\,U_{mf}$. The results are plotted in Figure 6, showing a similar behavior to he case for $G_{1,PCM} = 500$ l/min. The model predicts higher temperatures at all times, except for at $G_{2,PCM} = 375$ l/min after the phase change, where the emperatures predicted by the model are slightly lower than the experimental data.

[Figure 6 about here.]

4.1. Influence of the heating rate

To study the influence of the heating rate, charging experiments with the PCM at a low air heating rate of approximately 0.2°C/min are carried out. For this slow air heating rate, there is a low rate of heat accumulation in the distributor plate, which causes a negligible temperature difference (less than 0.5°C) between the gas in the plenum chamber and the gas at the bed inlet. Therefore, under these experimental conditions, T_{in} is not corrected, and its value is assumed to be equal to the temperature measured in the plenum chamber.

Figure 7 presents the temperature profiles for the PCM with a flow rate of $G_{1,PCM} = 500$ l/min and an air heating rate of 0.2°C/min. It is evident hat there is a better agreement between the experimental and numerical data.

[Figure 7 about here.]

The same experiments are repeated for flow rates of $G_{2,PCM} = 375$ l/min and $G_{3,PCM} = 675$ l/min, also obtaining good concordance between the experiments and the model. It can be seen that higher charging times are needed at lower flow rates.

For the low heating rates shown in this section, the experimental and numerical results present better agreement because the heating rate is similar to the 0.5°C/min applied in the DSC measurements for the determination of the enthalpy-temperature curves. This low heating rate assures thermal equilibrium in the sample introduced in the DSC.

[Figure 8 about here.]

4.2. Heat accumulation in the distributor plate

When the heating rate designed for the experiments is high and there is no possibility to experimentally characterize the influence of the distributor plate, the temperature of the air entering the bed can be estimated by introducing the energy balance equation for the distributor plate into the model. Neglecting convective heat transfer and assuming that the air leaves the distributor at the temperature of the distributor plate T_{dist} [20], the energy balance for the distributor plate yields the expression

$$m_{dist} c_{p,dist} \frac{dT_{dist}}{dt} = G \rho_a c_{p,a} \left(T_{plenum} - T_{dist} \right) + A_{dist} U_{dist} \left(T_0 - T_{dist} \right), \quad (17)$$

where m_{dist} and $c_{p,dist}$ are the mass and specific heat of the distributor plate, T_{plenum} is the temperature at the plenum chamber and A_{dist} is the heat transfer area between the distributor and the ambient environment. U_{dist} is the

heat transfer coefficient between the distributor and the ambient environment, given that the product $A_{dist}U_{dist} = 0.37$ W/K.

Non-dimensionalizing the Equation (17) using

$$\hat{T}_{dist} = \frac{T_{dist} - T_0}{T_{max} - T_0}, \quad \hat{T}_{plenum} = \frac{T_{plenum} - T_0}{T_{max} - T_0},$$

the result is

$$\frac{d\hat{T}_{dist}}{d\hat{t}} = R_{a-dist}\left(\hat{T}_{plenum} - \hat{T}_{dist}\right) + St_{dist-dist}\left(\hat{T}_0 - \hat{T}_{dist}\right). \tag{18}$$

The non-dimensional parameters R_{a-dist} and $St_{dist-dist}$ correspond to the expressions

$$R_{a-dist} = \frac{A\varepsilon H\rho_a c_{p,a}}{m_{dist}c_{p,dist}}, \qquad St_{dist-dist} = \frac{A_{dist}U_{dist}\varepsilon H}{m_{dist}c_{p,dist}U}.$$

The solution to Equation (18) is:

$$\hat{T}_{dist} = \left(\hat{T}_0 - \frac{b}{a}\right)e^{-a\hat{t}} + \frac{b}{a} \tag{19}$$

where $a = R_{a-dist} + St_{disto-dist}$ and $b = R_{a-dist}\hat{T}_{in} + St_{dist-dist}\hat{T}_0$.

When simulating experiments in which the heat accumulation in the distributor plate cannot be neglected, the temperature of the gas that leaves the distributor and enters the bed, T_{in}, can be significantly different from the temperature measured in the plenum chamber, T_{plenum}. Assuming that T_{in} has the same value as the distributor plate temperature, it can be calculated using Equation (19).

The comparison between the numerical results for the PCM charging process calculated using different methods to estimate the inlet air temperatures is presented in Figure 9, where the temperature measured in the plenum chamber is defined as T_{plenum}, and T_{exp} corresponds to the same experimental measurements presented in Figure 5 for the flow rate $G_{1,PCM} = 500$ l/min. The product $A_{dist}U_{dist} = 0.37$ W/K is estimated according to these experimental conditions. The numerical results of the dense phase temperature T_d are shown for the following methods: (i) $T_{d,1}$ is the result obtained if the inlet air temperature is taken as the temperature measured in the plenum chamber, (ii) $T_{d,2}$ is the result obtained if the inlet air temperature is taken as the distributor temperature calculated using equation (19) and (iii) $T_{d,3}$ is the result obtained if the inlet air temperature is experimentally determined by subtracting the temperature drop across the distributor from the temperature measured in the plenum chamber.

It is evident that the dense phase temperature, $T_{d,1}$, obtained using the temperature measured in the plenum chamber as an estimation of the inlet air temperature, is always higher than the experimentally measured temperature because the temperature drop across the distributor, which has a significant value at this heating rate, is not accounted for. By contrast, the results for $T_{d,2}$ and $T_{d,3}$, where the influence of the distributor is considered experimentally and numerically, are similar and agree well with the experimental measurements. This confirms that the temperature of the air entering the bed can be estimated numerically by including Equation (18) in the model proposed. The discrepancies found between the model and experimental results during the phase change process are due to the high heating

rate of the PCM at these experimental conditions, as explained before.

[Figure 9 about here.]

5. Conclusions

A numerical model for heat transfer in a fluidized bed with granular PCM material has been presented. The proposed non-dimensionalization of the energy equations results in the same differential equation system regardless of whether the granular material contains PCM. In this manner, the same numerical procedure can be used in cases with or without PCM. Furthermore, the model takes into account the energy stored in the wall and the air temperature drop across the distributor plate.

The comparison between the numerical and experimental data shows good agreement for the conventional material, sand. When there is a phase change in the granular material, the model properly predicts the experimental results if the heating rate of the bed is slow (0.2°C/min) because the enthalpy-temperature curve introduced in the model has been obtained in a DSC that also has a slow heating rate to ensure equilibrium conditions in the sample.

The solution of the distributor plate energy equation makes possible to properly estimate the inlet air temperature, whose value is significantly different from the gas temperature measured at the plenum chamber if the heating rate is high.

Acknowledgments

This work was partially funded by the Spanish Government (Project ENE2010-15403), the regional Government of Castilla-La Mancha (Project

PPIC10-0055-4054) and Castilla-La Mancha University (Project GE20101662).

6. Notation

A	cross sectional area of the bed [m^2]
c_p	specific heat [$J \cdot kg^{-1} \cdot K^{-1}$]
d	diameter [m]
G	volumetric flow rate [$m^3 \cdot s^{-1}$]
g	gravity [$m \cdot s^{-2}$]
H	height of the bed [m]
H_{bc}	heat interchange across the bubble cloud boundary per unit volume of bubble phase [$W \cdot m^{-3} \cdot K^{-1}$]
H_w	height of the wall [m]
h_b	convective heat transfer coefficient between the bubbles and the dense phase [$W \cdot m^{-2} \cdot K^{-1}$]
h_w	convective heat transfer coefficient between the dense phase and the container wall [$W \cdot m^{-2} \cdot K^{-1}$]
i	enthalpy [J]
k	thermal conductivity [$W \cdot m^{-1} \cdot K^{-1}$]
m	mass [kg]
P_b	perimeter of the cross sectional area of bubbles [m]
S_b	bubble surface [m^2]
St	Stanton number [-]
T	temperature [°C]
T_{pc}	phase change temperature [°C]
U	superficial gas velocity [$m \cdot s^{-1}$]
U_b	rising velocity of bubbles [$m \cdot s^{-1}$]

U_{dist}	heat transfer coefficient between the distributor and the ambient surroundings [W·m^{-2}·K^{-1}]
U_{mf}	minimum fluidization velocity [m·s^{-1}]
U_{wo}	global heat transfer coefficient between the container wall and the ambient surroundings [W·m^{-2}·K^{-1}]
V	bed volume [m^3]
V_b	bubble volume [m^3]

Greek symbols

ρ	density [kg·m^{-3}]
σ_{dp}	standard deviation of the mean particle diameter [m]
ε	voidage in the bed [-]
δ	volume fraction of bed consisting of bubbles [-]
Δt	time step [s]
Δx	spatial step [m]

Subscripts

0	ambient/initial
a	air
b	bubble
d	dense phase
$dist$	distributor
in	inlet
max	maximum value
p	particle
pc	phase change
s	solid

w	wall
wi	inner wall
wo	outer wall

References

[1] M. Farid, A. Khudhair, S. Razack, S. Al-Hallaj, A review on phase change energy storage: materials and applications, Energ. Convers. Manage. 45 (2004) 1597–1615.

[2] A. Benmansour, M. Hamdan, A. Bengeuddach, Experimental and numerical investigations of solid particles thermal energy storage unit, App. Therm. Eng. 26 (2006) 513–518.

[3] A. Regin, S. Solanki, J. Saini, An analysis of a packed bed latent heat thermal energy storage system using pcm capsules: Numerical investigation, Renew. Energ. 34 (2009) 1765–1773.

[4] M. Elsayed, I. Megahed, El-Refaee, Experimental testing of fluidized bes thermal storage, Sol. Wind Tech. 5 (1988) 15–25.

[5] Z. Sozen, J. Grace, K. Pinder, Thermal energy storage by agitated capsules of phase change material. 1 . pilot scale experiments., Ind. Eng. Chem. Res. 27 (1988) 679–684.

[6] M. A. Izquierdo-Barrientos, C. Sobrino, J. A. Almendros-Ibáñez, Thermal energy storage in a fluidized bed of pcm, Chem. Eng. J. 230 (2013) 573–583.

[7] K. Wagialla, A. Fakeeha, S. Elnashaire, A. Almaktary, Modeling and simulation of energy storage in fluidized beds using the two-phase model, Energ. Sourc. 13 (1991) 189–201.

[8] A. M. El-Halwagi, M. A. El-Rifai, M. M. El-Halwagi, Maximization of thermal efficiency of fluidized-bed heat regenerators, Heat Recov. Syst. CHP 11 (1991) 141–148.

[9] A. Faghri, Y. Zhang, in: A. Faghri, Y. Zhang (Eds.), Transport Phenomena in Multiphase Systems, Academic Press, Boston, 2006, pp. 1 – 106.

[10] D. Kunii, O. Levenspiel, Bubbling bed model for kinetic processes in fluidized plate. gas-solid mass and heat transfer and catalytic reactions., Ind. Eng. Chem. Proc. D.D. 7 (1968) 481–492.

[11] B. Kilkiş, Modeling the heat transfer coefficient between a surface and fixed and fluidized beds with PCM, Chem. Eng. J. 46 (1991) 47–60.

[12] M. A. Izquierdo-Barrientos, C. Sobrino, J. A. Almendros-Ibáñez, Modeling of the heat transfer coefficient in fixed and fluidized beds with pcm, in: Eurotherm Seminar 99: Advances in Thermal Energy Storage, Lleida.

[13] M. A. Izquierdo-Barrientos, C. Sobrino, J. A. Almendros-Ibáñez, Modeling the heat transfer coefficient between a surface and fixed and fluidized beds with PCM, Int. J. Heat Mass Transfer. Submited for publication (2014).

[14] M. A. Izquierdo-Barrientos, C. Sobrino, J. A. Almendros-Ibáñez, Heat transfer from immersed surfaces in fluidized beds: modeling and comparison with experimental data, Powder Technol. Submited for publication (2014).

[15] D. Kunii, O. Levenspiel, Fluidization Engineering, Butterworth-Heinemann, 1991.

[16] D. Geldart, Types of gas fluidization, Powder Technol. 7 (1973) 285–292.

[17] M. Rady, Study of phase changing characteristics of granular composites using differential scanning calorimetry, Energ. Convers. Manage. 50 (2009) 1210 – 1217.

[18] R. Darton, R. LaNauze, J. Davidson, D. Harrison, Bubble growth due to coalescence in fluidized beds, Trans. Inst. Chem. Eng. 55 (1977) 274–280.

[19] J. Davidson, D. Harrison, Fluidised particles, Cambridge University Press, 1963.

[20] J. Hoebink, K. Rietema, Drying granular solids in fluidized beds i: Description on basis of mass and heat transfer coefficients, Chem. Eng. Sci. 35 (1980) 2135–2139.

[21] P. Heertjes, H. de Boer, A. de Haas van Dorsser, Temperature and humidity measurements in a drying fluidized bed, Chem. Eng. Sci. 2 (1953) 97–107.

List of Figures

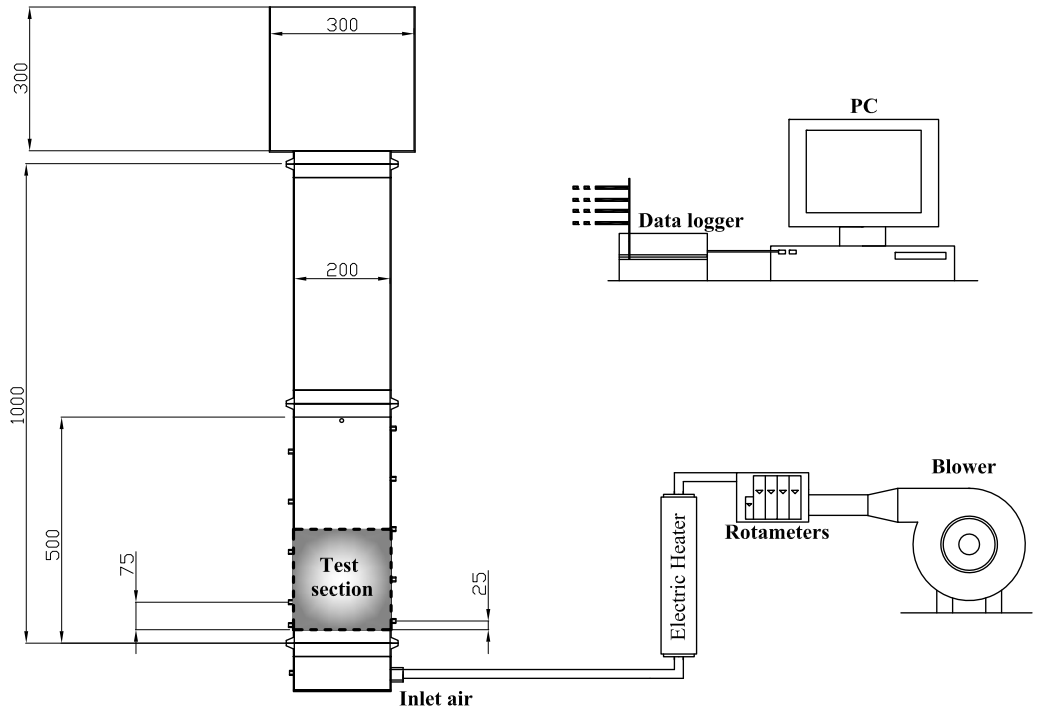

Figure 1: Schematic representation of the experimental apparatus. Dimensions in mm.

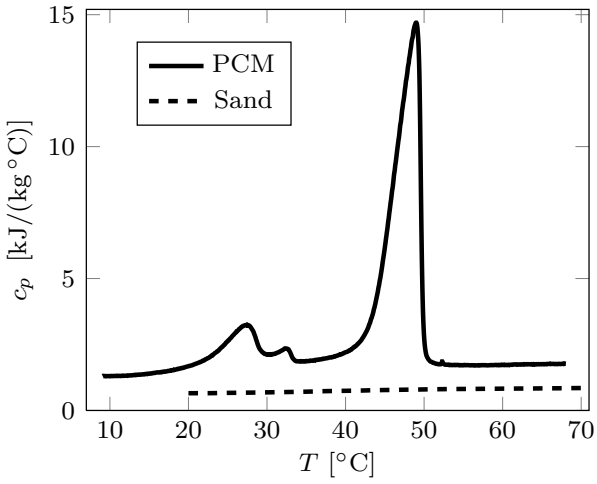

(a)

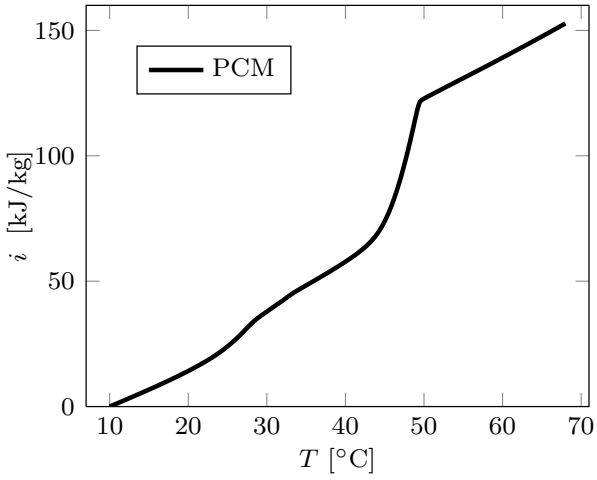

(b)

Figure 2: (a) Specific heat variation with temperature for the sand and the PCM (c_p=$\partial i/\partial T$) and (b) enthalpy variation with temperature for the PCM.

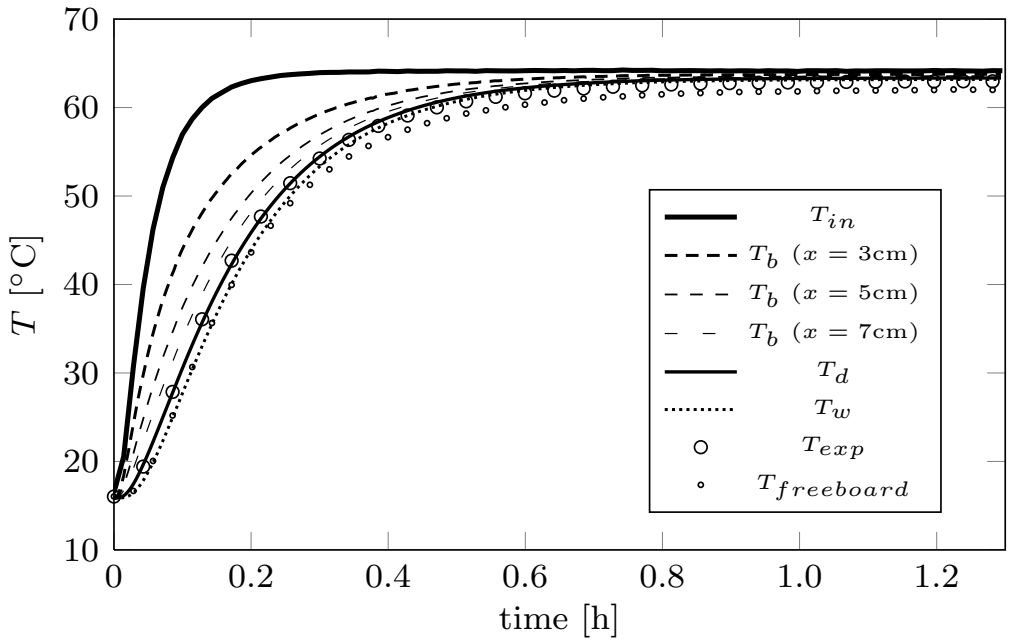

Figure 3: Temperature evolution of the inlet air T_{in}, the bubble phase at different heights T_b, the dense phase T_d, the temperature of the wall T_w, the experimental temperature of the dense phase T_{exp} and the temperature measured in the freeboard $T_{freeboard}$ when the bed is filled with sand and the flow rate is $G_{1,sand} = 1000$ l/min.

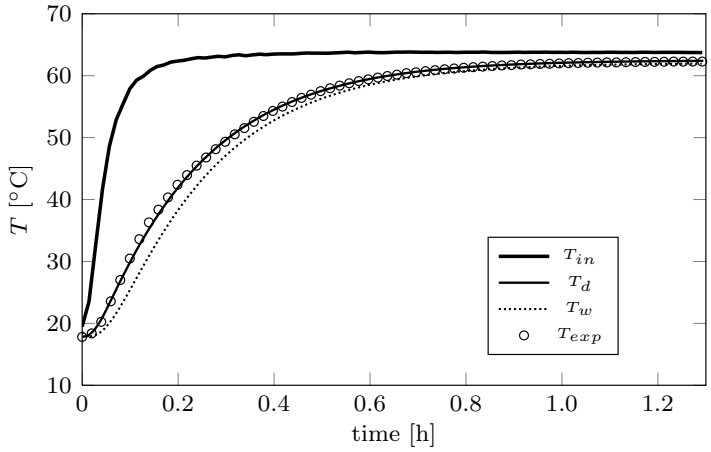

(a) $G_{2,sand} = 700$ l/min

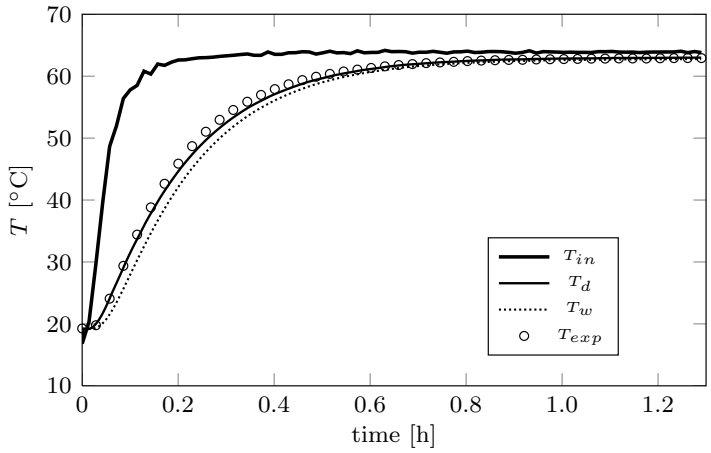

(b) $G_{3,sand} = 875$ l/min

Figure 4: Evolution of the inlet air temperature T_{in}, the dense phase temperature T_d, the temperature of the wall T_w and the experimental temperature of the dense phase T_{exp} for a flow rate of (a) $G_{2,sand} = 700$ l/min and (b) $G_{3,sand} = 875$ l/min when the bed is filled with sand.

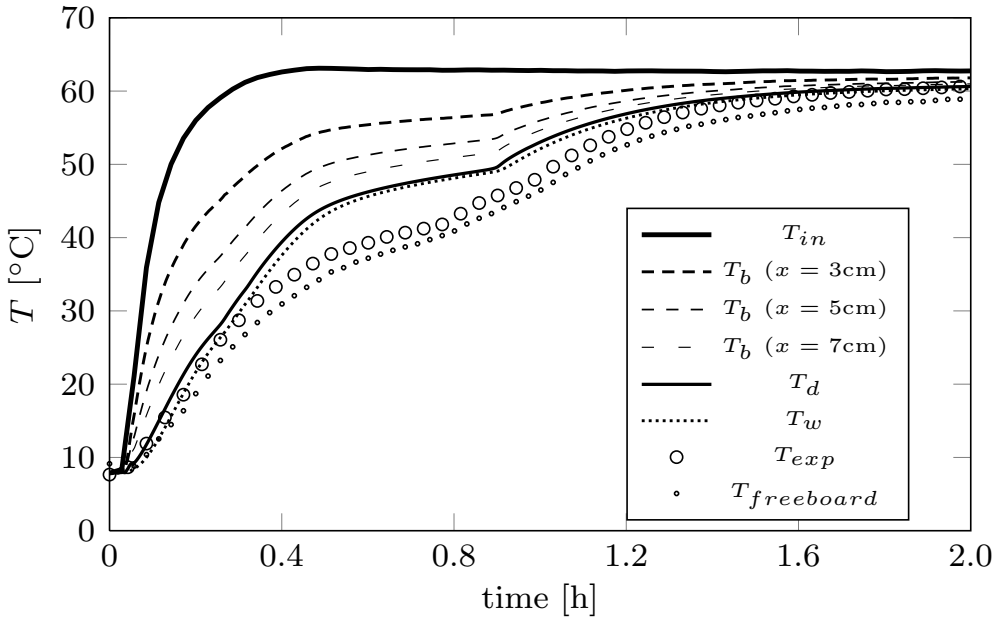

Figure 5: Temperature evolution of the inlet air T_{in}, the bubble phase at different heights T_b, the dense phase T_d, the temperature of the wall T_w, the experimental temperature of the dense phase T_{exp} and the temperature measured in the freeboard $T_{freeboard}$ when the bed is filled with PCM and the flow rate is $G_{1,PCM} = 500$ l/min.

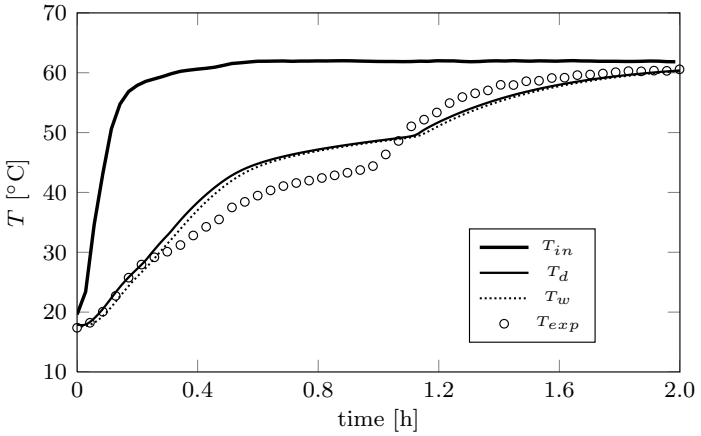

(a) $G_{2,PCM} = 375$ l/min

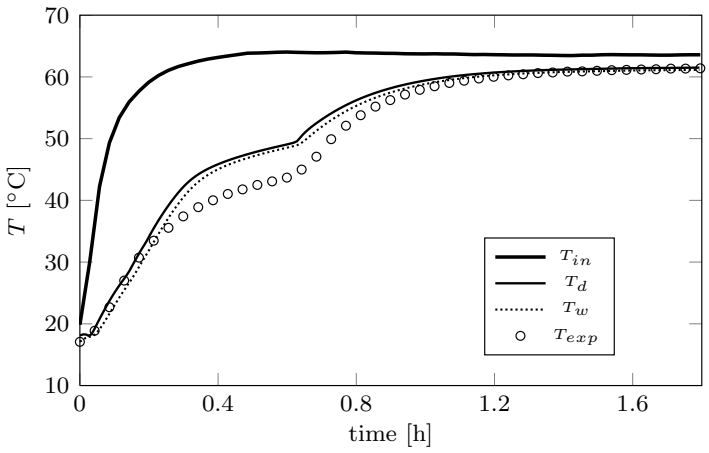

(b) $G_{3,PCM} = 625$ l/min

Figure 6: Evolution of the inlet air temperature T_{in}, the dense phase temperature T_d, the temperature of the wall T_w and the experimental temperature of the dense phase T_{exp} for a flow rate of (a) $G_{2,PCM} = 375$ l/min and (b) $G_{3,PCM} = 625$ l/min when the bed is filled with PCM.

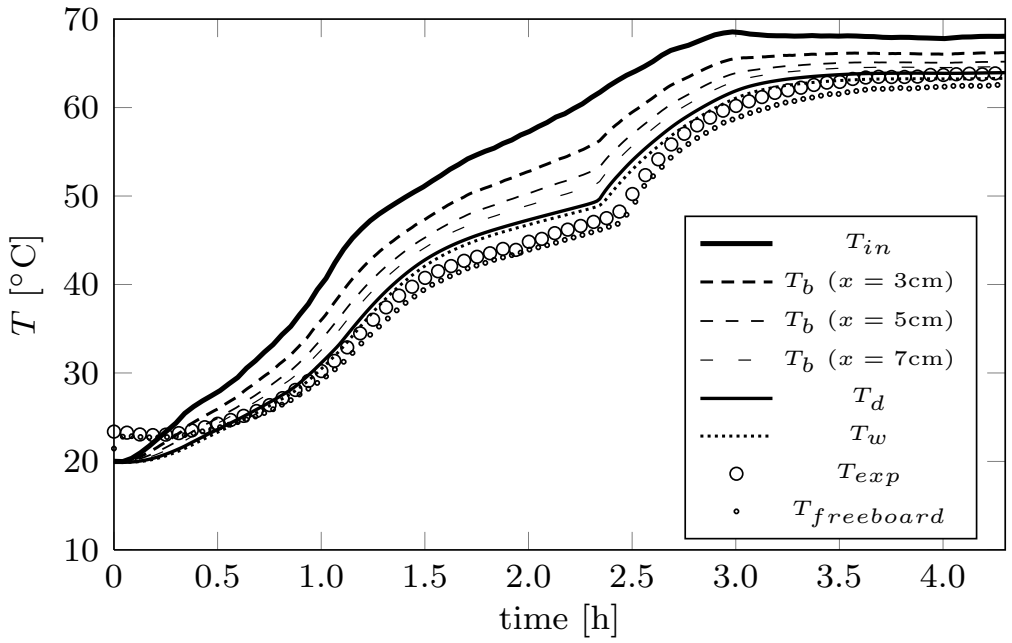

Figure 7: Temperature evolution of the inlet air T_{in} with a heating rate of 0.2°C, temperature of the dense phase T_d, temperature of the wall T_w, bubble phase temperature at different heights T_b, experimental temperature of the dense phase T_{exp} and temperature measured in the freeboard $T_{freeboard}$ when the bed is filled with PCM and the flow rate is $G_{1,PCM} = 500$ l/min.

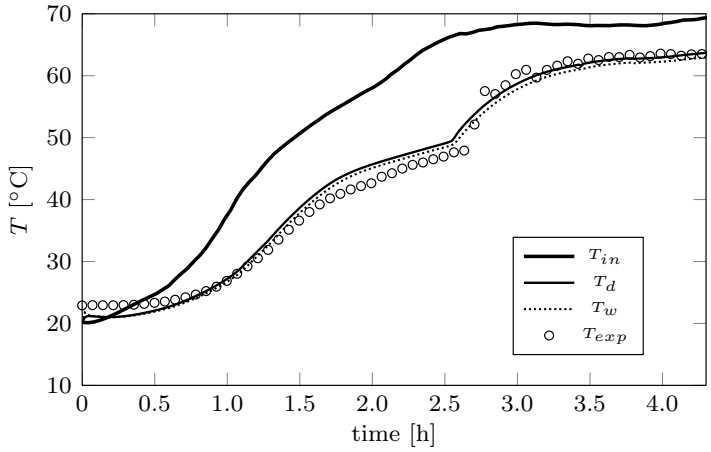

(a) $G_{2,PCM} = 375$ l/min

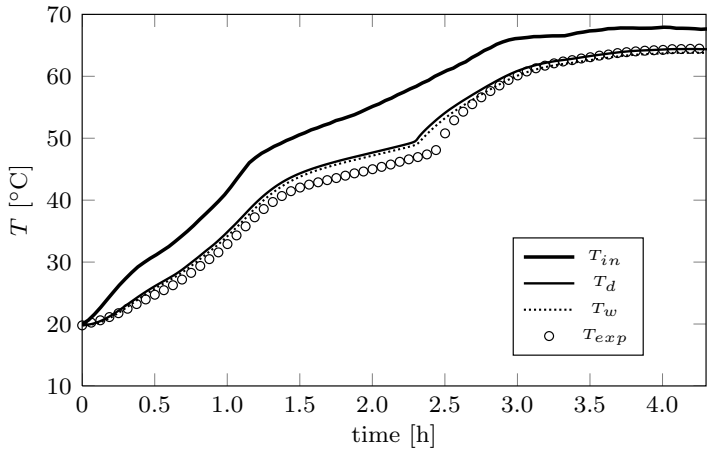

(b) $G_{3,PCM} = 625$ l/min

Figure 8: Temperature evolution of the inlet air T_{in} with a heating rate of 0.2°C, temperature of the dense phase T_d, temperature of the wall T_w and experimental temperature of the dense phase T_{exp} for a flow rate of (a) $G_{2,PCM} = 375$ l/min and (b) $G_{3,PCM} = 625$ l/min.

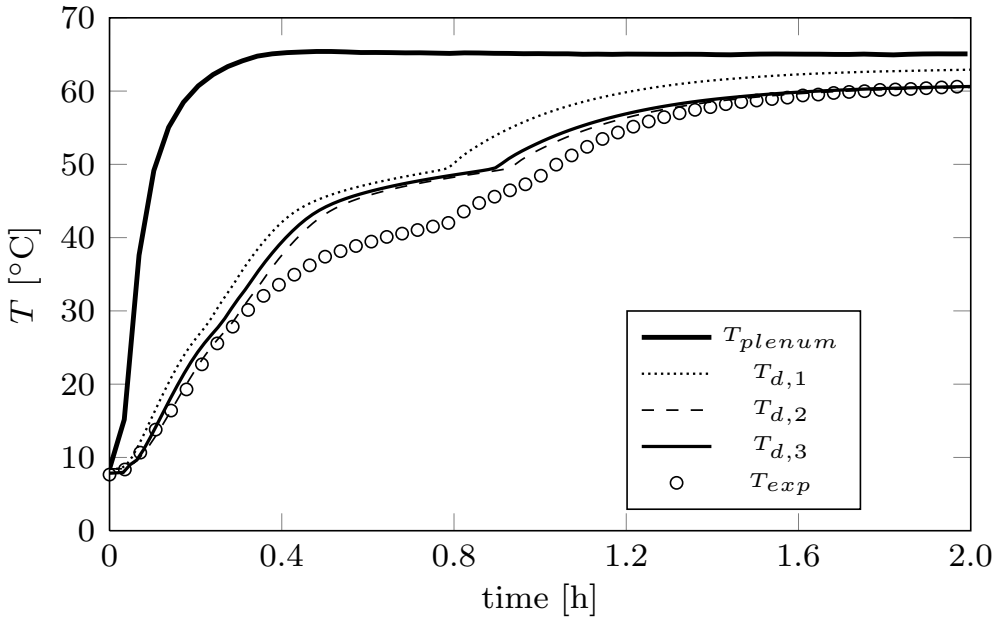

Figure 9: Temperature evolution of the air measured in the plenum chamber T_{plenum}, the dense phase temperature obtained by applying three different methods for the estimation of the inlet air temperature ($T_{d,1}$, $T_{d,2}$ and $T_{d,3}$) and the dense phase temperature measured experimentally (T_{exp}) when the bed is filled with PCM at a gas flow rate of $G_{1,PCM} = 500$ l/min.

List of Tables

Material	ρ [kg/m^3]	k [W/m·K]	$\overline{d}_p$ [mm]	σ_{dp} [mm]	U_{mf}[m/s]
Sand	2632.3	4.2	0.57	0.07	0.27
GR50	1550.5	4.0	0.54	0.08	0.13

Table 1: Properties of the materials studied.

Initial condition ($t = 0$)	Boundary condition ($x = 0$)
$T_d = T_b = T_w = T_0$	$T_b = T_{in}$

Table 2: Initial and boundary conditions for Equations (1), (7) and (8).

Initial condition ($\hat{t} = 0$)	Boundary condition ($\hat{x} = 0$)
$\hat{T}_d = \hat{T}_b = \hat{T}_w = 0$	$\hat{T}_b = 1$

Table 3: Dimensionless initial and boundary conditions for Equations (9), (10) and (11).

Sand			
G [l/min]	700	875	1000
h_w [W/(m^2 K)]	414	617	894
H_{bc} [W/(m^3 K)]	4.57×10^4	3.87×10^4	3.44×10^4
GR50			
G [l/min]	375	500	625
h_w [W/(m^2 K)]	520	560	600
H_{bc} [W/(m^3 K)]	2.94×10^4	2.22×10^4	1.89×10^4

Table 4: Values of the heat transfer coefficients h_w and H_{bc} for the different materials, temperatures and gas flows used in this work.